FTM2001-14, Version 8, October 26, 2001

Photometric and Astrometric Precision for the Descoped FAME: Stellar Temperature Effects, 10%-Astrometric Distance Limit

Rob Olling

USNO/USRA, Washington, DC

ABSTRACT

The attainable astrometric and photometric precision for an instrument such as FAME is a function of the number of photons detected. To first order the number of detected photons depends only on apparent magnitude of a star. This memo quantifies the correction to the 1^{st} order estimate due to the "color" or effective temperature (T_{eff}) of the stellar targets. That is to say, for a given magnitude limit in a given band, the attainable astro/photometric precision depends on T_{eff}. For stars with a given V-band magnitude, but for a wide range in effective temperature, I calculate the number photons that will be detected in the astrometric passband, as well as the ensuing astrometric and photometric errors. I also present a plot of the spectral energy distributions (SEDs) for a representative set of stars. To summarize: 1) A descoped FAME will be able to achieve the astrometric and photometric science goals for most stars, but only if the mission can be extended to approximately 5 years, and only for two of the four SDSS bands, 2) in the astrometric band, the single-measurement photometric precisions equals 2.2 and 47 mmag, at V=9 and V=15 (for a G2 star), 3) the average grid star is expected to yield about 50% more photons than an A0V star, 4) late M stars at $T_{eff} \lesssim 3,000$K are more than 2 to 3 magnitudes (≥ 6 times) brighter in the astrometric band than A0V stars with *identical* V-band magnitudes, 5) meaningful parallaxes can be obtained for late-type stars down to V=17 or 18, 7) for cool stars, the astrometric distance limit is about three times larger than would be predicted on the basis of the apparent magnitude in the V band, 8) about 30% of the FAME stars will have a parallax accuracy $\leq 10\%$, 9) about 42% of those stars with are K stars, and 10) 1-2 mas astrometry on stars brighter tna V=10.5 is possible for background levels $\lesssim 2.3$ ke$^-$ per unbinned pixel. *This memo employs an updated value for the overall throughput of the system: 50% as compared to 75% used in earlier memos.*

1. Introduction

Synthetic spectra with fixed surface gravity [$log(g)$=4.5, i.,e., Main Sequence] and metallicity ($[Fe/H] = 0$, i.e., Solar abundance) were selected from the database generated by Le Jeune *et al.* (1997, A&AS,125, 229). Two sets of the spectra were analyzed: the original and corrected version. The latter is more realistic for in the low temperature regime whereas the corrections to the hot models are small. These spectra were converted into a photon spectrum (photons/cm^2/sec/nm) and folded with "the" overall FAME throughput and quantum-efficiency curve. It is *assumed* that the average overall throughput equals 50% in the 550-850 nm region. This QE*TP curve is tabulated in table 1, and is thought to be relevant for the start of the mission, and may be only 44% (13% worse) after 5 years.

Table 1: As a function of wavelength (1^{th} column), this table presents the assumed efficiency of FAME (2^{nd} column). The efficiency (f_S) tabulated in the 2^{nd} row is assumed to be equal to the product of the quantum efficiency (QE) and the throughput (TP) of the FAME telescope. The low throughput at 370 nm is caused by an absorption feature of the silver coatings of the mirrors. The average value in th 550-850 nm region equals 50%. The 3^{rd} row lists what is believed to be a reasonable lower limit as to the mission-end efficiencies (f_E).

λ [nm]	350	370	400	450	500	550	600	650	700	750	800	850	900	950	1000
$f_S(\lambda)$	0.13	0.00	0.32	0.48	0.55	0.56	0.56	0.55	0.53	0.48	0.43	0.35	0.25	0.12	0.01
$f_E(\lambda)$	0.05		0.35		0.40		0.45		0.40		0.25		0.15		0.05

2. Results

So as to determine the number of photons in a particular photometric or astrometric band, the following bandpass shape is assumed:

$$B(\lambda) \;=\; \exp\left(-\tfrac{1}{2}\left(\frac{\lambda-\lambda_0}{\sigma}\right)^8\right) \qquad (1)$$

where λ_0 is the central wavelength and the full-width at half maximum ($FWHM$) equals 2.075σ. This function is chosen so as to have 100% central throughput[1] and rather steep filter edges: the full-width at quarter maximum is approximately 10% larger than $FWHM$.

Several publications are used as sources of stellar spectra templates. For A0V stars, I use the "a0v.dat" file from Pickles (1998, PASP, 110, 863; P98, hereafter) library. Many of

[1]Note that "real" filters often have a somewhat wiggly response curve and $\lesssim$ 97% peak throughput. Here we neglect the wavy nature of the filter response and assume that the overall throughput value (50%) includes filter losses.

Pickles' stars have a wavelength range from 115 to 1062 nm, and are normalized at 555.6 nm. To convert the P98 flux units (ergs/sec/cm^2/Å) to photons/sec/cm^2/nm, I multiply by 10x(λ/555.6). I take the normalization at 555.6 nm from Tug *et al.*(1977, A&A, 61, 679) to be 9700 photons/sec/cm^2/nm for Vega. Finally, to connect the photon counts to a magnitude scale, I assume that Vega has V=0.03, so that a zeroth magnitude A0V star yields 9972 photons/sec/cm^2/nm an 555.6 nm.

Given the assumptions enumerated above, it is possible to calculate the expected number of photons that FAME will detect in a given bandpass. I perform these calculations for three different bandpasses: 1) the band formed by the QExTP curve from table 1, 2) a 400 to 900 nm band (BROAD), and 3) the 550-850 nm band (NARROW). The first bandpass yields the maximum possible number of photo-electrons, the second bandpass was standard for the CSR-FAME, while the last bandpass is the default for the descoped FAME. The results are listed in table 2 below. In this table, I list value for two designs of the FAME instrument: A) the design as described in the CSR [dubbed "FAME Classic" (FC)], and B) the descoped design, or "FAME Light" (FL). It is assumed that the mirror dimensions for FAME Classic and FAME Light are 53x13 and 40x9 cm^2, respectively. The integration time per transit were taken to be: 1.56 and 1.56/0.7=2.23 seconds, for FC and FL, respectively[2].

Table 2: The expected number of photo-electrons for a 9^{th} magnitude A0V star in the original and descoped design for three different bandpasses. The average QE*TP value for FAME Classic equals 75% and 50% for FAME Light. Employ columns #6 and #7 from table 7 to obtain the photon counts for different spectral types. Note that only about 93% of these photo-electrons are located inside the standard FAME raster of 13x24 pixels.

band	Classic	Light	FC(13x24)	FL(13x24)
QExTP	876,683	436,831	815,315	406,253
QExTP x 400-900	791,811	394,541	736,384	366,923
QExTP x 550-850	402,605	200,609	374,423	**186,566**

Not all stars of the "same" apparent magnitude yield an equal number of photo-electrons. To first order, the number of photo-electrons is determined by the apparent magnitude and effective temperature of the star. Extinction, surface gravity and metallicity also play a role, but their effects are not considered here. Temperature effects are discussed below.

[2]Note that FL's overall QE*TP is only 66.7% of that for FAME Classic, and that the FAME CSR design (the wide-open FL case) had 4.4 times more photons than the current FAME design (the narrow FL case).

2.1. T_{eff} Effects

In figure 1, I present the spectra of the models described in the Introduction. All spectra are normalized such that they have *identical* photon counts in the V band. Note that most spectral lines are located in the blue part ($\lambda \lesssim 550$ nm) of the spectrum for stars hotter than 4,500K. That is to say, spectral classification relies heavily on "blue" bands.

In the discussion below I will only consider the 400-900 and 550-850 nm astrometric bands. The broad band basically covers the whole range plotted in figure 1, while the narrower, redder band lies between the normalization point (V band) and the wavelength of the reddest "dip" in the T_{eff}=2,500K spectrum. Given these SEDs, I determine, as a function of T_{eff}, how many photons will be detected in either astrometric band, given that *all models have identical photon counts (magnitude) in the V band.* The results are presented in table 7. The last two columns are the relative photon counts, i.e., normalized by the photon counts of a T_{eff}=9,400K star.

3. Astrometry & Photometry: Magnitude and T_{eff} scaling

Given some simplified assumptions regarding the FAME PSF, it is possible to estimate the achievable astrometric and photometric accuracy and precision. I determine the single-measurement precision in a manner similar to the procedure described in FTM2001-03: A) Fitting is performed on one-dimensional images, B) the PSF is assumed to be a pixel-integrated Gaussian with a FWHM of 1.41 pixels, C) an additional smearing due to 1.45 pixel TDI-mismatch[3] is included, D) the employed PSF has a FWHM of approximately 1.73 pixels[4], E) a single Gaussian function is fitted to all PSFs, F) fits are made for a number (30) of PSF locations within a single pixel (30 pixel-phases), G) at each pixel-phase, 50 random profiles are fitted that include Poisson noise, readnoise and 14-bit digitization effects, H) the fit precisions is assumed to be the RMS of the ensemble of all pixel-phase and noise-realizations (1500 per magnitude), I) steps A)-H) are repeated for a range of magnitudes. The procedure A)-I) also yields estimated of the photometric precision.

The results are listed in tables 8-25 below. Conceptually, these tables are split in four groups. The first group (8-10) summarizes the results for the narrow astrometric band. The second group (12-13) is for the SDSS bands. The last two groups (14-25) present the astrometric and photometric results in more detail.

---

[3]This smearing is assumed to be pillbox like: width=1.41 pixels, and an RMS width of $1.45/\sqrt{12} = 0.42$ pixels).

[4]i.e., close to the width of a pillbox-smeared polychromatic PSF for a G2 star with FWHM=1.68 pixels.

For the narrow band results, each table is calculated for the following effective temperatures: 9400, 8000, 6500, 5777, 4500, 4000, 3500 and 3000 K. Some tables list the number of photo-electrons ($N_{e,tot}$), which are calculated as follows: 1) take 367.8 ke$^-$ for a V=9 A0V star in the narrow astrometric band [cf. table 2], 2) multiply by the photon-enhancement factor [7^{th} column of table 7], 3) apply an apparent magnitude correction [multiply by 2.512^{9-V}], 4) determine the astrometric precision via the equation:

$$\delta x_0^P \sim \left(6.410^{-4} + \frac{0.58}{\sqrt{N_{e,tot}}} + \frac{16}{N_{e,tot}} \right) \qquad \text{[pixels]}. \tag{2}$$

Equation (2) has been derived[5] from the simulations for an A0V star, and can be used to obtain results for other cases without detailed numerical evaluation. Note that equation (2) does not take the T_{eff}-dependent broadening of the PSF into account. The coefficients are accurate to about 6%. FAME is in the photon-statistic regime when the 1^{th} term of equation (2) dominates. At lower flux levels, FAME is in the readnoise regime, where the $1/N_{e,tot}$ term dominates. Inspection of tables 8-25 shows that the readnoise-dominated regime starts between V=13 and V=14 for A0V stars, and around V=15 for M5 stars.

The single-measurement **precision** (δx_0^P) is meant to include random errors only, whereas the **accuracy** (δx_0^A) includes limitations due to systematic effects that can not be calibrated.

For most astrophysical applications, the most interesting quantities are position, parallax, and proper motion (and their errors), not the one-dimensional error. Some tables below enumerate the achievable parallax errors, where $\delta\pi$-relation is derived from Murison's (2001) detailed simulations for a with a sun angle of 35^o , a 20 days precession period, a 40 min spin period, 11 astrometric chips, a single-measurement accuracy of δx_0^A= 840 μas, and a 1.1 degree field of view. From Murison's results[6], I find that $\delta\pi$ is given by:

$$\delta\pi \approx 2.02 \frac{\delta x_0^A}{\sqrt{N_{obs}}} , \tag{3}$$

where on average 1982 observations are obtained during the 5 years of operation.

Finally, I also present the attainable photometric precision for the single-measurement and mission-end cases, respectively. The numerical experiments described above also yield an estimate for the single-measurement photometric *precision*, and its dependence on the

---

[5]Note that this relation is slightly different from versions 7 and earlier. This change does not affect any conclusions drawn in this memo.

[6]From Murison's table, I derive these ($N_{obs}, \delta\pi_{\mu\text{as}}$) pairs: (879, 60.0), (1484, 45.0),(1764, 41.4),(4617, 18.4).

total number of detected photons. I find:

$$\delta V \sim 0.51 + \frac{831}{\sqrt{N_{e,tot}}} + \frac{20,237}{N_{e,tot}} \pm 0.15 \qquad \text{[mmag]}, \tag{4}$$

where the coefficients are probably uncertain by about 6%. In the astrometric band, this yields δV= 2.6 (57) mmag at V=9 (15) for an A0V star. For a G2 star these numbers are 2.2 and 47 mmag, and twice smaller for a M5 star. Assuming that the system can be calibrated perfectly, the system performs about 44.5 ($= \sqrt{N_{obs}} = \sqrt{1982}$) times better at mission-end, to yield *precisions* of 0.06 (1.4) mmag at V=9 (15) for an A0V star. These photometric results for the astrometric bandpass represent best-possible cases, since it is assumed that a perfect instrumental calibration can be established.

Equation (4) is also applicable to observations in an SDSS band. To tolerably good approximation (at the moment), the number of photons in either SDSS band (r' or i') will equal the number of photons in the astrometric band, multiplied by the bandwidth ratio (=130/300=0.433). For a G2 star, these considerations lead to a single-measurement *precision* of 3.6 and 100 mmag at V=9 and V=15, respectively. (cf. table 13) in an SDSS band. Given that there will be about 180 observations per filter at mission-end, the final SDSS photometric *precision* will be 0.3 and 8.3 mmag at V=9 and V=15, for a G2 star.

3.1. Photometric Filters & Astrometry

If the SDSS photometric filters will be used for astrometry, the results will be degraded due to their narrower bandwidths. In tables 22-25, I present the astrometric and photometric results, for a limited number of T_{eff}'s. A summary of these results is presented in tables 12 and 13. To arrive at the numbers in these tables, I assume that only *one* CCD is used per filter, so that the number of observations equals: $N_{obs,SDSS}$ = 1982x1/11 = 180. Furthermore, I assume that the number of photons per SDSS filter is given by the bandwidth ratio with respect to the 550-850 astrometric band: 130/300=0.433. For the SDSS filters, the astrometric precision is also calculated via equation (2).

Thus, to first order, for a given magnitude, the astrometry from a photometric chip will have a single-measurement precision that is about 1.52 ($=1/\sqrt{0.433}$) times worse than that of the unfiltered chips. Alternatively, SDSS filters saturate about at magnitudes about 0.9 magnitudes brighter than the unfiltered CCDs.

4. Astrometric and Photometric Precision & Accuracy

The astrometric and photometric precision expressed via equations (2) and (4) above and the tables 8 through 25 below only include degradation due to photon statistics, readnoise

and digitization. However, there are other effects that will adversely affect the final achievable accuracies. Some of these effects, as communicated by Hugh Harris, are:

1. CCD defects, such as charge traps, possibly growing during mission,
2. QE variations across CCDs and varying with time not modeled correctly,
3. CCD linearity not modeled correctly,
4. Incorrect PSF, leading to incorrect aperture corrections,
5. Errors in the estimated sky background (including scattered light),
6. Non-Gaussian or inflated CCD read noise.

The corrections due to these effects are currently uncertain, because presently we have no data and little guidance for estimating magnitude of the effects quantitatively. These photometric degradation occur mostly at faint magnitudes because the readnoise and the determination of the sky background are least certain in the faint regime. Harris estimates photometric degradation factors of 1.2 for V$\lesssim$13, 1.4 at V=14, 1.6 at V=15 and 1.8 at V=16 in the astrometric band. Because the photometric filter is narrower than the astrometric filter, these correction factors are down-shifted by about 0.90 magnitudes in the SDSS bands.

In the following subsections, I evaluate the effects of the last three effects enumerated above. Currently, the first three effects can not be modeled accurately. Some comments are in order, though. @1) Low temperatures and charge injection mitigate the effects due to charge traps. @2) Time and position variation of the CCD's response can and should be monitored and modeled using bright stars: these effects are not magnitude dependent. @3) non-linearities should be modeled by using a progressively larger number of calibration stars towards the faint magnitudes. Further modeling and test data are required to estimate the magnitude of the effects.

From the discussion below, it follows that effects that degrade the photometry will also degrade the astrometry. Thus, the estimated photometric degradation factors would also apply to the astrometry (see below). However, at some level, photometry will be easier than astrometry since the former entails just photon *counting*, whereas photon *location* is most important for astrometry.

4.1. PSF Effects

In FTM2001-11, I found that about 7% of the total flux is missing from the default FAME raster (13x24 pixels) and a sinc^2 PSF. The amount of missing flux is a function of

stellar effective temperature (r'-i'), in-scan smearing and cross-scan smearing. Similar numbers are expected for the real FAME PSF. In FTM2001-11, I conclude that photometric errors resulting from a PSF-mismatch vary slowly with smearing, but show a ±0.3% dependency on stellar effective temperature. The effects of smearing/PSF-mismatch must be calibrated by employing measurements in rasters that are larger than the standard (13x24). However, the aperture correction must be applied to both the fluxes and their errors, so that their ratio and hence the apparent magnitude error is unaffected.

Astrometric and photometric accuracy are degraded due the loss of the photons that fall outside of the box. These losses are already included in the precision calculations (cf table 2).

4.2. Background Level Effects

I have estimated the downgrading of the photometric precision due to a DC background level. The results (from PSF fitting) are tabulated in table 3. This table list the astrometric precision and degradation factors as a function of background level ans stellar brightness. The photometric degradation factors are approximately equal to the astrometric degradation factors and are not listed separately (see also section 4 and figure 9 of FTM2001-09)

4.2.1. Faint Background Levels

There are at least four sources of background light: 1) scattered light from the Earth, Moon, Planets and bright stars, 2) large galaxies, 3) diffuse Galactic nebulae, and 4) Zodiacal light. @2) Nearby (spiral) galaxies have an upper limit to the V-band central surface brightness of about 19.5 mag/arcsec^2 [cf., de Jong, 1994, A&AS, 104, 179]. @3) A sample of supernova remnants, planetary nebulae and diffuse nebulae from the Messier catalog yields an average surface brightness of 21.7 ±2 mag/arcsec^2. @4) The maximum surface brightness of the Zodiacal light, as observed by FAME, would be 22.5 mag/arcsec^2 (490 S_{10} at an elongation of 55^o), whereas a more typical number would be 200 S_{10} (Frey *et al.*, 1974, A&A, 36, 447). These surface brightness values correspond to 3.7, 0.6 ±4, 0.88 and 0.3 photo-electrons per unbinned-descoped pixel, respectively. Inspecting table 3, we see that the largest DC backgrounds due to extended sources (3.7 e$^-$/2Dpixel) yields a degradation of only about 10% (14%) at V=15 (V=16). A more typical background level due to Zodiacal light is 0.3 electrons/2Dpixel results in photometric and astrometric degradations of just 1 % (4%) at V=15 (V=16).

4.2.2. Bright Background Levels

FAME's baffling system will be designed to minimize the effects of scattered light to a level better than 3.2 10^{-9} ergs/s/pixel (2362 e^- per unbinned pixel) further than 25 degrees from the Earth (TBR). At this level, astrometric *precision* for stars of V=9, 10 and 11 is 2.1, 2.15, and 2.90 times worse than without background. However, the *accuracy* is less affected: to 1.2/350, 2.0/350 and 4.0/350 parts of a pixel.

4.3. Readnoise Effects

I have also investigated the effects of readnoise (RN) on the achievable astrometric and photometric precision. In table 4 below, I enumerate the astrometric and photometric results for a G2 star. I have used several RN levels: $\frac{1}{2}$, $1\frac{1}{2}$, and 2 times the default level of RN=12 e^-. At V=13, the precision at RN=6, 24, and 36 is about 94%, 109%, and 120% of that at RN=12. For V=15, these numbers become: 75%, 122%, and 150%.

Readnoise effects are particular important for objects beyond the standard faint limit of V=15: at V=18, I find a 59%, 131% and 157% RN effect. From this discussion it follows that faint object science will benefit (suffer) greatly from a reduction (increase) in the readnoise level. At this point, it is unclear what to expect for the variation in readnoise levels. However, a 50% variation seems excessive.

4.4. Precision Degradation: Summary

The conclusion is that when using PSF fitting techniques, astrometric and photometric precision are affected in the same manner: an X% degradation of one quantity implies an X% degradation of the other quantity. Because of its photon-*counting* nature, aperture photometry is less sensitive to processes that change the shape of the PSF than centroiding.

Effects due to DC background levels and uncertainties are expected to be small in the majority of circumstances. A 50% uncertainty in the knowledge of the readnoise level corresponds to a 7% change in precision at V=13, and a 25% change at V=15, for astrometry and photometry.

More theoretical and laboratory investigations into the behavior of the CCDs and the consequences for the astrometric and photometric precision/accuracy are needed.

5. Effects on the Limiting Distance

In section 2.1, I discussed how stellar effective temperature affects the expected photon counts. Below I will investigate some of the consequences for astrometry and astrophysics.

In the top panel of figure 2, I converted the photon counts as tabulated in table 7 to magnitude differences. In the bottom panel of that figure, I present the scaled distance out to which a given relative distance error is achieved: $D(T_{eff})/D(A0V) = \sqrt{2.512^{\Delta m}}$. This relation is not entirely correct at the faint end, because the astrometric errors increase more rapidly than photon statistics suggests (cf., eqn. 2). For the lower panel of figure 2, I converted the effective temperature to absolute magnitude using the main-sequence relation. The three curves in each panel of figure 2 represent the following:

1. full, black curve: number of photons in the 400-900 band, normalized by the counts for an A0V star *in the 550-850 band*.
2. dashed, black curve: number of photons in the 400-900 band, normalized by the counts for an A0V star in the 400-900 band.
3. dashed, red curve: number of photons in the 550-850 astrometric band, normalized by the counts for an A0V star *in the 550-850 band*.

Case 1 is presented to illustrate, from a photon-statistics perspective, the effects of using a narrow rather than the broad bandpass: 1) for the hottest stars, the narrow astrometric bandpass reduces the number of photons by a factor of about two, 2) for cool stars, the 550-850 astrometric band yields only 30% less photons than the 400-900 band.

Comparing case 2 and 3, we see that $N_\nu(T_{eff})$ varies less for the 400-900 nm band than for the 550-850 nm astrometric band. This is so because cool stars emit many photons in the red region and little in the blue part, while hot stars have few photons in the red and many photons ion the blue part of the spectrum (see figure 1). In either of the cases, the coolest stars are 2.5 to 3.5 magnitudes brighter in the astrometric band than an A0V star.

5.1. Photon-Count Corrected Distance Limits

In figure 3, I present a contour plot (straight black lines) of the stellar distance as a function of apparent magnitude ($m_V = V$, horizontal axis) and absolute magnitude (M_V, vertical axis):

$$d \;=\; 10^{(V-M_V+5)/5}. \qquad [pc] \tag{5}$$

In the same figure, I over-plot the photon-count corrected distances as the curved (red) lines.

The results presented in the previous sections indicate that the X%-distance limit is substantially larger for late-type stars than for early-type stars with identical V-band magnitudes. For example, an $M_V \sim 10.5$ star with $m_V = 15$ is located at $d \sim 80$ parsec. According to V-band photon-statistics, FAME's parallax error would be 585μ-arcsec. However, due to their extra photon-yield, such $M_V = 10.5$ stars will still have a 585μ-arcsec precision at a

distance of about 160 pc. As a result, about eight $[(160/80)^3]$ the number of late-M stars with good parallaxes could be as large as 2 10^6.

It is interesting to compare the distances from eqn. (5) with an astrometric distance limit. I define the $X\%$- distance limit as the distance at which the mission-end parallax error equals $X\%$. If we consider a 10% distance error, FAME's 585 μ-arcseconds parallax error at V=15 for an A0 star yields a limiting distance of $D_{10\%} = 171$ parsec. $D_{X\%}$ increases towards brighter apparent magnitudes approximately according to photon statistics, but in the relations below, I also include the effects due to read-nose limitations:

$$d_{X\%} \;=\; 17.1\ \alpha(V)\ X_{\%}\ , \qquad [pc] \qquad (6)$$

$$\alpha(V) \;\equiv\; \frac{\delta x_0^A(V=15)}{\delta x_0^A(V)} \;=\; \frac{\delta x_0^P(V=15)}{MAX(\,1/350,\ \delta x_0^P(V,PEF)\,)} \qquad (7)$$

where X is expressed in percent, and $\alpha(V)$ is a factor that describes the magnitude-dependent astrometric accuracy, δx_0^A is the photon-count dependent astrometric accuracy [cf, eqn. (2)] which has an lower limit of $1/350^{th}$ of a pixel. The $\delta x_0^P(V, PEF)$ term accounts for the varying number of electrons with stellar effective temperature [via the photon-enhancement factor (PEF) as tabulated in table 7], as well as the photon-statistics and read-noise effects.

One can define the $X\%$ astrometric distance limit, d_{AXL}, as the intersection between equations (5) and (6). For given PEF and M_V values, this limiting distance will occur at different apparent magnitudes, V_{AXL}. For stars that lie beyond their d_{AXL}, FAME will be photon-limited, so that the parallax error will be worse than $X\%$. At smaller distances, the distance error will be better than $X\%$.

In figure 3, I have over-plotted the contour of the 10%-astrometry distance (as the jagged line[s]). In this figure, the part of the diagram that is contoured with dashed lines lies beyond the astrometric limit. For these stars it may still be possible to determine accurate photometric parallaxes (see FTM2001-15).

6. Astrometric Distance Limits for the FAME Catalog

From the expected distribution of stars in the FAME catalog, it is possible to estimate what fraction of stars will be astrometry limited. Sean Urban estimated the fraction of FAME stars that have a given spectral type and luminosity class. I copy these numbers to table 5 below, and add the corresponding absolute magnitudes, PEF factor, and 10%-astrometry limiting distances and apparent magnitudes.

From table 5 it follows that the FAME catalog will contain quite a few intrinsically bright stars that are located beyond the limiting distance. For example, all AV stars beyond about

1051 parsec, with apparent magnitudes V∈[12,15], will be so far away that their parallax errors will exceed 10%. Also note that table 5 enumerates *main-sequence stars only*, which comprise about 83% of the FAME catalog.

To estimate how many stars lie beyond d_{A10L}, I assume that the number of stars increase proportional to d^2 (proportional to surface area of the Galactic disk, not disk volume [this estimate will be a lower limit]). The maximum distance out to which a star will end up in the FAME catalog is found by substituting V=15 in equation 5, I find:

$$d_{MAX}(15, M_V) \;=\; 10^{((15-M_V+5)/5)} \qquad \text{[pc]} \tag{8}$$

Thus, the total of the number of stars in the FAME catalog, divided by the number of stars with good parallaxes is given by:

$$F_{T/G}(M_V) \;=\; \left(\frac{d_{MAX}}{d_{AXL}(M_V)}\right)^2 \tag{9}$$

So that the fraction of stars with good astrometry is given by:

$$f_{dX\%} \;=\; \frac{1}{F_{T/G}(M_V)} \;=\; \left(\frac{d_{AXL}(M_V)}{d_{MAX}}\right)^2 \tag{10}$$

Employing equations (8) and (10), I find that 37.5% of the main-sequence stars in the FAME catalog will have their distances measured to 10%, or better. In practice, one also has to consider the effects due to interstellar extinction. Along the average line of sight, one can expect about 1 magnitude of extinction (in the V band) per kilo-parsec. This effect can be incorporated by changing the "V" factor in equation (5) by "$V - A_{V,kpc} \times d/1000$", where $A_{V,kpc}$ is the extinction per kpc. Equation (5) then becomes non-linear but can be solved numerically. I present detailed results in table 6 below. As we can see from table 6, the effects of interstellar extinction are not very large. This is so because most stars (i.e., F and G stars) are at a distance of 400-600 pc, so that extinction effects are not very significant. In both cases, roughly 37% of the main-sequence (∼13 million) stars will have a measured parallax with $\delta\pi/\pi \lesssim 0.1$. Note that stars with accurate parallaxes are of later type than the catalog as a whole. For example, the catalog contains only 14% K stars, while 42% of stars with $\delta\pi/\pi \lesssim 0.1$ will be K stars.

6.1. Faint-FAME versus TYCHO-2

For the remaining 63% of the main-sequence stars (21 million), FAME's current baseline will yield proper motions and a single color: r'-i'. Some experiments in Galactic astrometry will be very difficult to perform with such a limited data set. This subset of stars with poor astrometry can be compared with the Tycho catalog, which also tabulates proper

motions and one color (B-V). However, contrary to the Tycho catalog, the FAME catalog *will* contain parallax measurements, albeit of "poor" quality. Researchers who are interested in performing experiments on the sample of 21 million FAME stars with poor parallaxes might test their methodologies on the Tycho-2 catalog.

I also estimate the parallax accuracy that can be obtained with a photometric filter system as proposed for the FAME Classic mission. The results (FTM2001-15) are promising but lie outside the scope of the current FAME baseline.

7. Conclusions

For the descoped FAME mission, the attainable 5-year astrometric *precision* for A0 stars equals 27 and 585 μ-arcseconds at V=9 and V=15. Assuming a lower limit to the single-measurement *accuracy* of $1/350^{th}$ of a pixel, we get 38 and 585 μ-arcseconds for the same magnitudes. Compared with the requirements laid out in the Science Requirements Document (SRD), these values are slightly better at the bright end, and slightly worse for faint stars.

The single-measurement photometric *precision* in the astrometric band for the descoped mission is about 2.2, 8.3 and 47 mmag at V=9, V=12 and V=15, for a G2 star.

A single-measurement precision of about 1-2 mas is attaianble for stars brighter than V=10.5 at a stray-light background level of 2.3k e^- per 2D pixel [12.24 mag/(4 pixels), 3.2 10^{-9} ergs/se/2Dpixel].

Neither the photometric nor the astrometric precision suffers significantly due to the light levels of extended sources such as the Zodiacal light, Galactic nebulae or spiral galaxies.

For the SDSS filters, the photon yield is only 43% of the astrometric filter, so that the following single-measurement (SM) precisions are obtained at V=(9;15): (3.9;109), (3.6;102) and (2.6;75) mmag for A0, G2 and M2 stars. The mission-end (ME) precisions are, at V=(9;15): (0.3;8.5),(0.3;8.0) and (0.2;5.8) mmag for the same spectral types.

Checking the precisions in the astrometric and SDSS bands against the SRD requirements, I find the following conflicts:

- **Solar Neighborhood Stars, wide:** Requires SM accuracy of 10 mmag at V=15, Available: 57 mmag precision for A0, 23 mmag for M5
- **Galactic Structure, wide:** Requires 1 mmag SM accuracy at V=5-9, Available: 2.7 mmag precision for A0, 1.0 mmag for M5
- **All, SDSS:** No SDSS photometry will be available in the V=5=8 range

Because the SRD requirement on SDSS photometry for the SM *accuracy* is close to the photon-statistics SM precision, the photometric data reduction requires special attention.

The ME *photometric precision in the astrometric band* is significantly better than the required ME *accuracy* (e.g., 0.2 mmag versus 2 mmag at V=12; 1.3 versus 8 at V=15). Thus, there is quite a bit of room for calibration residuals in the ME photometry in the astrometric band. For the SDSS bands, there is substantially less room for uncalibrated residuals, especially at faint magnitudes. At V=9,12,15, I find the following (requirement;available precision) pairs: (1.0;0.3), (2.0;1.2), (8.0;8.5) for A0 stars and (1.0;0.2), (2.0;0.8), (8.0;5.7) for M2 stars.

For the narrow astrometric band, astrometry and photometry will be about $\sqrt{15} \sim 3.8$ times better for late M stars than for A0 stars. Solar-type stars have about 50% more photons than A0 stars of identical V magnitude. Thus, cool stars down to m_V=18 will yield enough photons for a meaningful parallax determination ($\Delta\pi/\pi \lesssim 0.1$ for $d \lesssim 100$ pc).

Stars in the red clump or higher up the giant branch (B-V$\gtrsim$ 0.95) have more than twice the number of photons than main-sequence stars of similar absolute magnitude (i.e., A-type and earlier stars). Also, for stars in the Tycho-2 catalog (with V $\in [8.5, 11]$ and $\overline{\mathrm{B-V}}$=0.57), I estimate a photon-yield increment of 1.53 with respect to A0V stars of similar magnitudes. Thus, the photon yield of an average Tycho-2 star is equal to that of a G2-G4 star (cf., table 7).

Note that all calculations in this document are performed at start-of-mission sensitivities. At mission end, the detected number of photons may be 40% smaller. Assuming that the degradation is linearly over time, the average number of photons detected is 85% of what assumed in this document, so that the "average" astrometric and photometric errors may be $\sqrt{1/0.85}$ =1.08 times worse than reported here.

Substantially better performance can be achieved for faint objects if the read noise can be reduced to RN=6 e^- per binned pixel: down to 80% and 57% of the RN=12 values.

About 63% of the FAME catalog will have a parallax accuracy worse than 10%. About 40% of the stars with good parallax accuracy are K stars, or later.

I also estimate the parallax accuracy that can be obtained with a photometric filter system as proposed for the FAME Classic mission. The results (FTM2001-15) are promising but lie outside the scope of the current FAME baseline.

Table 3: This table comprises two parts. The top part gives the absolute values of the single-measurement astrometric precision (in mas) as a function of the background level. The bottom half tabulates the degradation factors (the values scaled by the "no-background" values), which are approximately equal to the astrometric degradation factors. The asterisks indicate that the peak signal-to-noise level has dropped below three. The background level is listed in the first three columns: #1 the surface brightness (mag) per 4 unbinned pixels, and #2 and #3 the number of electrons/1000 per unbinned and binned pixel(s). The other columns list the precisions or degradation factors for several stellar V-magnitudes. A total number of 275.7k electrons is assumed for the V=9 case (G2 star). The readnoise was 12 e^- per 1D pixel. At low background levels, the reported errors are fluctuating due to the Monte Carlo procedure. The bold-faced row at $V_{BG4} = 12.24$ corresponds to a background level of 3.2 10^{-9} ergs/s/2Dpixel.

V_{BG4} $\frac{mag}{4pix}$	BG_{2D} ke^-	BG_{1D} ke^-	9	10	11	12	13	14	15	16
8.00	117.00805	2808.19312	3.73	7.86	21.36	53.37	***	***	***	***
9.00	46.57963	1117.91113	2.67	4.85	12.72	34.28	79.82	***	***	***
10.00	18.54285	445.02832	2.06	3.21	7.82	21.98	55.37	***	***	***
11.00	7.38171	177.16093	1.73	2.30	4.96	13.70	36.50	82.25	***	***
12.24	**2.36228**	**56.69484**	1.05	1.53	3.19	7.95	20.63	50.27	***	***
13.00	1.16982	28.07558	1.14	1.34	2.28	5.34	14.11	36.36	80.69	***
14.00	0.46569	11.17658	0.79	1.02	1.74	3.76	9.17	22.84	52.40	***
15.00	0.18539	4.44928	0.53	0.82	1.46	2.94	6.43	14.81	34.05	69.08
16.00	0.07380	1.77121	0.48	0.73	1.24	2.30	4.63	9.95	22.37	47.17
17.00	0.02938	0.70510	0.47	0.71	1.15	2.01	3.76	7.51	15.99	33.81
18.00	0.01170	0.28069	0.47	0.69	1.09	1.83	3.28	6.24	12.65	26.53
19.00	0.00466	0.11174	0.48	0.71	1.10	1.79	3.08	5.61	10.79	21.95
20.00	0.00185	0.04448	0.54	0.75	1.11	1.75	2.93	5.22	9.90	19.86
22.00	0.00029	0.00705	0.51	0.73	1.09	1.73	2.89	5.09	9.52	18.83
26.00	0.00001	0.00018	0.48	0.71	1.10	1.77	2.96	5.15	9.41	18.11
8.00	117.00805	2808.19312	7.77	11.07	19.42	30.15	***	***	***	***
9.00	46.57963	1117.91113	5.56	6.83	11.56	19.37	26.97	***	***	***
10.00	18.54285	445.02832	4.29	4.52	7.11	12.42	18.71	***	***	***
11.00	7.38171	177.16093	3.60	3.24	4.51	7.74	12.33	15.97	***	***
12.24	**2.36228**	**56.69484**	2.18	2.15	2.90	4.49	6.97	9.76	***	***
13.00	1.16982	28.07558	2.38	1.89	2.07	3.02	4.77	7.06	8.57	***
14.00	0.46569	11.17658	1.65	1.44	1.58	2.12	3.10	4.43	5.57	***
15.00	0.18539	4.44928	1.10	1.15	1.33	1.66	2.17	2.88	3.62	3.81
16.00	0.07380	1.77121	1.00	1.03	1.13	1.30	1.56	1.93	2.38	2.60
17.00	0.02938	0.70510	0.98	1.00	1.05	1.14	1.27	1.46	1.70	1.87
18.00	0.01170	0.28069	0.98	0.97	0.99	1.03	1.11	1.21	1.34	1.46
19.00	0.00466	0.11174	1.00	1.00	1.00	1.01	1.04	1.09	1.15	1.21
20.00	0.00185	0.04448	1.13	1.06	1.01	0.99	0.99	1.01	1.05	1.10
22.00	0.00029	0.00705	1.06	1.03	0.99	0.98	0.98	0.99	1.01	1.04
26.00	0.00001	0.00018	1.00	1.00	1.00	1.00	1.00	1.00	1.00	1.00

Table 4: Astrometric & Photometric Precision as a function of apparent magnitude and readnoise (RN). Column #1 lists the magnitude, the remaining ones list three sets of δx_0 and δV for the case that RN equals $\frac{1}{2}$, 1, $1\frac{1}{2}$, and 2 times the FAME default value (12 e^-).

	RN= 6		RN=12		RN=18		RN=24	
V	δx_0 [mas]	δV [mmag]	δx_0 [mas]	δV [mmag]	δx_0 [mas]	δV [mmag]	δx_0 [mas]	δV [mmag]
12	1.75	8.11	2.01	8.29	2.20	8.62	2.35	9.10
13	2.70	13.22	2.82	14.07	3.00	15.32	3.25	16.94
14	4.40	20.83	4.74	23.61	5.32	27.51	6.12	32.34
15	7.56	36.23	9.37	46.87	11.64	59.43	14.31	73.46
16	13.81	65.43	20.69	95.65	28.13	126.01	35.74	156.12
17	26.53	122.14	46.42	195.84	64.45	262.48	80.94	326.48
18	54.11	236.41	96.09	396.13	129.64	520.73	155.49	624.22

Table 5: Expected Contents and properties of the FAME catalog. Columns #1 through #5 list the spectral type and luminosity class (#1), effective temperature (#2), percentage of stars in the FAME catalog (#3), absolute magnitude (#4), and photon enhancement factor (#5). The last two columns list the 10%-astrometry limiting distance (#6) and apparent magnitude (#7). The last two columns were determined without considering the effects of interstellar extinction.

SP	T_{eff} [K]	C_f [%]	M_V [mag]	PEF	d_{A10L} [pc]	V_{A10L} [mag]
(1)	(2)	(3)	(4)	(5)	(6)	(7)
B5V	15,000	5	-1.2	1.00	2,000	10.31
A5V	8,300	7	1.9	1.08	1,051	12.01
F5V	6,600	24	3.5	1.31	748	12.87
G5V	5,600	28	5.1	1.48	517	13.67
K5V	4,200	14	7.4	2.20	318	14.91
M2V	3,500	5	10.0	3.25	176	16.23

Table 6: For main-sequence stars of spectral type (#1), several parameters derived from the **10%-astrometry criterion** are tabulated. Columns (#2)-(#7) is for the case of zero interstellar extinction, columns (#8)-(#13) is valid for the case of 1 magnitude extinction per kpc. The 10% distance (#2 & #8), the 10% apparent magnitde (#3 & #9), the maximum distance (#4 & #10), the ratio of the total number of stars to the number of stars with 10% parallaxes (#5 & #11), the fraction of stars with a parallax measurement better than 10% (#6 & #12), and the expected total number of stars ($= 4 \times 10^7\, C_f\, f_{dX\%}$) in #7 and #13. See section 6 for further details.

SP	d_{AXL} [pc]	V_{AXL} [mag]	d_{MAX} [pc]	$F_{T/G}$	$f_{dX\%}$ [%]	$N_{dX\%}$ [x1000]	d_{AXL} [pc]	V_{AXL} [mag]	d_{MAX} [pc]	$F_{T/G}$	$f_{dX\%}$ [%]	$N_{dX\%}$ [x1000]
(1)	(2)	(3)	(4)	(5)	(6)	(7)	(8)	(9)	(10)	(11)	(12)	(13)
B5	2,000	10.31	17380	75.5	1.3	26	1501	11.18	8706	33.6	3.0	59
A5	1,051	12.01	4169	15.7	6.4	178	854	12.41	2813	10.8	9.2	258
F5	748	12.87	1995	7.1	14.1	1350	638	13.16	1487	5.4	18.4	1767
G5	517	13.67	955	3.4	29.3	3281	459	13.87	773	2.8	35.3	3955
K5	318	14.91	331	1.1	91.9	5149	294	15.03	294	1.0	100.0	5600
M2	176	16.23	176	1.0	100.0	2000	168	16.30	168	1.0	100.0	2000

Table 7: The number of observable counts in the broad (3^{rd} column) and narrow (4^{th} astrometric bands as a function of effective temperature (1^{st} column). The approximate spectral type is listed in column #2. All models would have the same number of counts in the V band (3^{rd} column). The 6^{th} and 7^{th} columns are the counts in the broad and narrow bands, normalized by the appropriate Vega-like models at T_{eff} =9,400K. Note that the counts in columns # 3, #4 and #4 can be compared directly. Column #6 should be used to scale the photon counts in the broad astrometric band as listed in the 2^{nd} row of table 2 to get the total counts at a given T_{eff}. Likewise, use #c7 together with #r3.

T_{eff} (1)	Sp-type (2)	$N(V)$ (3)	$N(F_B)$ (4)	$N(F_N)$ (5)	$N_{nV}(F_B)$ (6)	$N_{nV}(F_N)$ (7)
2500	-	1.0	45.82	31.60	11.60	15.73
3000	M5	1.0	17.74	13.21	4.49	6.57
3500	M2	1.0	8.55	6.53	2.16	3.25
4000	K7	1.0	6.59	5.06	1.66	2.52
4500	K3	1.0	5.36	3.96	1.35	1.97
5000	K2	1.0	4.80	3.35	1.21	1.67
5500	G4	1.0	4.64	3.12	1.17	1.55
5777	G2 (Sun)	1.0	4.50	2.97	1.14	1.48
6000	G0	1.0	4.43	2.85	1.12	1.41
6500	F6	1.0	4.27	2.65	1.08	1.31
7000	F2	1.0	4.16	2.48	1.05	1.23
7500	F1	1.0	4.09	2.35	1.03	1.16
8000	A7	1.0	4.05	2.25	1.02	1.12
9000	A2	1.0	3.97	2.08	1.00	1.03
9400	A0 (Vega)	1.0	3.95	2.01	**1.00**	**1.00**
10000	B9	1.0	3.92	1.98	0.99	0.98
12000	B8	1.0	3.94	1.92	0.99	0.95
15000	B5	1.0	3.95	1.88	1.00	0.94
20000	B1	1.0	3.96	1.83	1.00	0.91
40000	O7	1.0	4.00	1.74	1.01	0.87

Table 8: The *single-measurement* **astrometric accuracy** in units of mas as a function of apparent magnitude (1^{th} column) for the spectral types listed in the first row (or T_{eff} as listed in the 2^{nd} row). This table is valid for the **narrow astrometric band**, and is constructed from the 5^{th} columns of tables 14-21 below.

V	A0	A7	F6	G2	K3	K7	M2	M5
-	9,400	8,000	6,500	5,777	4,500	4,000	3,500	3,000
(1)	(2)	(3)	(4)	(5)	(6)	(7)	(8)	(9)
8	0.84	0.84	0.84	0.84	0.84	0.84	0.84	0.84
9	0.84	0.84	0.84	0.84	0.84	0.84	0.84	0.84
10	0.86	0.84	0.84	0.84	0.84	0.84	0.84	0.84
11	1.31	1.24	1.15	1.09	0.96	0.86	0.84	0.84
12	2.12	1.99	1.83	1.72	1.48	1.31	1.16	0.85
13	3.64	3.39	3.09	2.87	2.43	2.12	1.84	1.29
14	6.65	6.15	5.53	5.10	4.24	3.63	3.11	2.07
15	12.90	11.85	10.55	9.65	7.86	6.62	5.57	3.54
16	26.54	24.21	21.34	19.37	15.49	12.84	10.62	6.44
17	55.14	50.01	43.74	39.44	31.06	25.38	20.68	12.01
18	166.52	146.93	123.47	107.76	78.15	59.14	44.27	19.95

Table 9: The *mission-end* **parallax accuracy** in units of mas as a function of apparent magnitude (1^{th} column) for the spectral types listed in the first row This table is valid for the **narrow astrometric band**, and is constructed from the 8^{th} columns of tables 14-21 below. A 5 year mission with 1982 astrometric observations is assumed.

V	A0	A7	F6	G2	K3	K7	M2	M5
-	9,400	8,000	6,500	5,777	4,500	4,000	3,500	3,000
(1)	(2)	(3)	(4)	(5)	(6)	(7)	(8)	(9)
8	0.038	0.038	0.038	0.038	0.038	0.038	0.038	0.038
9	0.038	0.038	0.038	0.038	0.038	0.038	0.038	0.038
10	0.039	0.038	0.038	0.038	0.038	0.038	0.038	0.038
11	0.060	0.056	0.052	0.049	0.044	0.039	0.038	0.038
12	0.096	0.090	0.083	0.078	0.067	0.059	0.053	0.039
13	0.165	0.154	0.140	0.130	0.110	0.096	0.084	0.058
14	0.302	0.279	0.251	0.232	0.192	0.165	0.141	0.094
15	0.585	0.538	0.479	0.438	0.357	0.300	0.253	0.161
16	1.204	1.098	0.968	0.879	0.703	0.583	0.482	0.292
17	2.502	2.269	1.985	1.790	1.409	1.151	0.938	0.545
18	7.555	6.667	5.602	4.889	3.546	2.683	2.009	0.905

Table 10: The *single-measurement* **photometric precision** in units of mmag as a function of apparent magnitude (1^{th} column) for the spectral types listed in the first row (or T_{eff} as listed in the 2^{nd} row). This table is valid for the **narrow astrometric band**, and is constructed from the 9^{th} columns of tables 14-21 below.

V	A0	A7	F6	G2	K3	K7	M2	M5
-	9,400	8,000	6,500	5,777	4,500	4,000	3,500	3,000
(1)	(2)	(3)	(4)	(5)	(6)	(7)	(8)	(9)
8	1.68	1.59	1.47	1.38	1.20	1.06	0.93	0.66
9	2.65	2.51	2.32	2.18	1.89	1.67	1.47	1.04
10	4.12	3.89	3.60	3.39	2.94	2.60	2.29	1.61
11	6.32	5.97	5.52	5.20	4.51	3.99	3.51	2.47
12	10.07	9.52	8.81	8.29	7.19	6.36	5.60	3.94
13	17.10	16.16	14.95	14.07	12.21	10.80	9.52	6.70
14	28.66	27.10	25.08	23.61	20.50	18.14	15.99	11.27
15	56.75	53.70	49.75	46.87	40.74	36.10	31.85	22.50
16	115.38	109.33	101.46	95.72	83.44	74.10	65.51	46.48
17	233.95	222.30	207.04	195.83	171.69	153.13	135.94	97.36
18	465.20	444.16	416.33	395.67	350.57	315.29	282.11	205.78

Table 11: The *mission-end* **photometric precision** in units of mmag as a function of apparent magnitude (1^{th} column) for the spectral types listed in the first row This table is valid for the **narrow astrometric band**, and is constructed from the 10^{th} columns of tables 14-21 below. A 5 year mission with 11 chips and 1982 astrometric observations is assumed.

V	A0	A7	F6	G2	K3	K7	M2	M5
-	9,400	8,000	6,500	5,777	4,500	4,000	3,500	3,000
(1)	(2)	(3)	(4)	(5)	(6)	(7)	(8)	(9)
8	0.038	0.036	0.033	0.031	0.027	0.024	0.021	0.015
9	0.060	0.056	0.052	0.049	0.042	0.038	0.033	0.023
10	0.093	0.088	0.081	0.076	0.066	0.058	0.051	0.036
11	0.142	0.134	0.124	0.117	0.101	0.090	0.079	0.056
12	0.227	0.215	0.199	0.187	0.162	0.143	0.126	0.089
13	0.387	0.366	0.338	0.318	0.276	0.244	0.215	0.151
14	0.652	0.616	0.570	0.536	0.465	0.411	0.362	0.254
15	1.308	1.236	1.143	1.075	0.932	0.824	0.726	0.510
16	2.731	2.581	2.386	2.245	1.946	1.721	1.516	1.066
17	5.848	5.527	5.111	4.810	4.170	3.688	3.248	2.285
18	12.967	12.257	11.338	10.670	9.255	8.187	7.212	5.078

Table 12: The *single-measurement* **astrometric accuracy [columns (2)-(5)]** and the *mission-end* **parallax accuracy [columns (6)-(9)]** in units of mas as a function of apparent magnitude (1^{th} column) for the spectral types listed in the first row (or T_{eff} as listed in the 2^{nd} row). This table is valid for an **SDSS band**, and is constructed from the 5^{th} and 7^{th} columns of tables 22-25 below. A 5 year mission with 180 photometric observations is assumed.

V	A0	G2	K3	M2	A0	G2	K3	M2
-	9,400	5,777	4,500	3,500	9,400	5,777	4,500	3,500
(1)	(2)	(3)	(4)	(5)	(6)	(7)	(8)	(9)
8	0.84	0.84	0.84	0.84	0.127	0.127	0.127	0.127
9	0.84	0.84	0.84	0.84	0.127	0.127	0.127	0.127
10	1.24	1.16	1.07	0.87	0.186	0.175	0.162	0.132
11	1.99	1.85	1.69	1.33	0.300	0.279	0.255	0.200
12	3.45	3.17	2.86	2.17	0.519	0.478	0.430	0.326
13	6.38	5.82	5.18	3.79	0.960	0.876	0.780	0.570
14	12.65	11.43	10.05	7.11	1.903	1.720	1.512	1.069
15	26.59	23.84	20.74	14.22	4.001	3.588	3.121	2.140
16	56.44	50.29	43.39	29.02	8.493	7.568	6.530	4.367
17	112.94	100.21	85.97	56.48	16.996	15.081	12.937	8.500

Table 13: The *single-measurement* [columns (2)-(5)] and *mission-end* **photometric precision [columns (6)-(9)]** in units of mmag as a function of apparent magnitude (1^{th} column) for the spectral types listed in the first row (or T_{eff} as listed in the 2^{nd} row). This table is valid for an **SDSS band**, and is constructed from the 9^{th} and 10^{th} columns of tables 22-25 below. A 5 year mission with 180 photometric observations is assumed.

V	A0	G2	K3	M2	A0	G2	K3	M2
-	9,400	5,777	4,500	3,500	9,400	5,777	4,500	3,500
(1)	(2)	(3)	(4)	(5)	(6)	(7)	(8)	(9)
8	2.52	2.36	2.17	1.71	0.188	0.176	0.162	0.128
9	3.90	3.65	3.36	2.65	0.291	0.272	0.250	0.198
10	6.14	5.75	5.29	4.18	0.459	0.430	0.395	0.312
11	9.80	9.18	8.44	6.68	0.733	0.687	0.631	0.499
12	16.52	15.48	14.23	11.27	1.239	1.161	1.067	0.843
13	29.28	27.45	25.25	20.01	2.209	2.069	1.901	1.503
14	53.08	49.79	45.84	36.40	4.045	3.789	3.483	2.754
15	108.94	102.35	94.40	75.30	8.503	7.966	7.322	5.793
16	217.99	205.39	190.12	152.97	17.838	16.715	15.370	12.169
17	438.82	415.68	387.32	316.85	39.555	37.089	34.130	27.070

On the following pages, the astrometric and photometric precision are tabulated for the **narrow astrometric band**.

Table 14: Expected Astrometric and Photometric precision and accuracies for A0 stars *in the 550-850 nm band.* The first two columns magnitude and total number of photo-electrons. The 3^{rd} and 4^{th} columns list the *single-measurement* **precision** (δx_0^P) in units of milli-arcseconds and fractions of a pixel. The 5^{th} and 6^{th} columns list the *single-measurement* **accuracy** (δx_0^A), assuming a best case accuracy of $1/350^{th}$ of a pixel. The 7^{th} and 8^{th} columns enumerate the corresponding achievable parallax errors (see § 3). The photometric **precision** for the *single-measurement* and *mission-end* cases is listed in #9 and #10. A 5 year mission with 1982 astrometric observations on 11 chips is assumed.

V	$N_{e,tot}$	$\delta x^P_{0,S}$	$\delta x^P_{0,S}$	$\delta x^A_{0,S}$	$\delta x^A_{0,S}$	$\delta\pi^P$	$\delta\pi^A$	δV_S	δV_M
	ke$^-$	mas	1/pix	mas	1/pix	mas	mas	mmag	mmag
(1)	(2)	(3)	(4)	(5)	(6)	(7)	(8)	(9)	(10)
8	467.87	0.45	655.1	0.84	350.0	0.020	0.038	1.68	0.038
9	186.28	0.60	487.4	0.84	350.0	0.027	0.038	2.65	0.060
10	74.20	0.86	340.7	0.86	340.7	0.039	0.039	4.12	0.093
11	29.56	1.31	224.0	1.31	224.0	0.060	0.060	6.32	0.142
12	11.78	2.12	138.7	2.12	138.7	0.096	0.096	10.07	0.227
13	4.70	3.64	80.9	3.64	80.9	0.165	0.165	17.10	0.387
14	1.87	6.65	44.3	6.65	44.3	0.302	0.302	28.66	0.652
15	0.75	12.90	22.8	12.90	22.8	0.585	0.585	56.75	1.308
16	0.30	26.54	11.1	26.54	11.1	1.204	1.204	115.38	2.731
17	0.12	55.14	5.3	55.14	5.3	2.502	2.502	233.95	5.848
18	0.06	166.52	1.8	166.52	1.8	7.555	7.555	465.20	12.967

Table 15: Expected Astrometric and Photometric precision and accuracies for A7 stars *in the 550-850 nm band.* For further details, see the caption of table 14.

V	$N_{e,tot}$	$\delta x^P_{0,S}$	$\delta x^P_{0,S}$	$\delta x^A_{0,S}$	$\delta x^A_{0,S}$	$\delta\pi^P$	$\delta\pi^A$	δV_S	δV_M
	ke$^-$	mas	1/pix	mas	1/pix	mas	mas	mmag	mmag
(1)	(2)	(3)	(4)	(5)	(6)	(7)	(8)	(9)	(10)
8	524.02	0.44	676.4	0.84	350.0	0.020	0.038	1.59	0.036
9	208.63	0.58	507.1	0.84	350.0	0.026	0.038	2.51	0.056
10	83.11	0.82	357.2	0.84	350.0	0.037	0.038	3.89	0.088
11	33.10	1.24	236.7	1.24	236.7	0.056	0.056	5.97	0.134
12	13.19	1.99	147.6	1.99	147.6	0.090	0.090	9.52	0.215
13	5.26	3.39	86.7	3.39	86.7	0.154	0.154	16.16	0.366
14	2.09	6.15	47.8	6.15	47.8	0.279	0.279	27.10	0.616
15	0.84	11.85	24.8	11.85	24.8	0.538	0.538	53.70	1.236
16	0.33	24.21	12.2	24.21	12.2	1.098	1.098	109.33	2.581
17	0.14	50.01	5.9	50.01	5.9	2.269	2.269	222.30	5.527
18	0.07	146.93	2.0	146.93	2.0	6.667	6.667	444.16	12.257

Table 16: Expected Astrometric and Photometric precision and accuracies for F6 stars *in the 550-850 nm band*. For further details, see the caption of table 14.

V	$N_{e,tot}$	$\delta x^P_{0,S}$	$\delta x^P_{0,S}$	$\delta x^A_{0,S}$	$\delta x^A_{0,S}$	$\delta\pi^P$	$\delta\pi^A$	δV_S	δV_M
	ke^-	mas	1/pix	mas	1/pix	mas	mas	mmag	mmag
(1)	(2)	(3)	(4)	(5)	(6)	(7)	(8)	(9)	(10)
8	612.91	0.42	706.0	0.84	350.0	0.019	0.038	1.47	0.033
9	244.02	0.55	535.0	0.84	350.0	0.025	0.038	2.32	0.052
10	97.20	0.77	380.9	0.84	350.0	0.035	0.038	3.60	0.081
11	38.72	1.15	254.9	1.15	254.9	0.052	0.052	5.52	0.124
12	15.43	1.83	160.7	1.83	160.7	0.083	0.083	8.81	0.199
13	6.15	3.09	95.4	3.09	95.4	0.140	0.140	14.95	0.338
14	2.45	5.53	53.2	5.53	53.2	0.251	0.251	25.08	0.570
15	0.98	10.55	27.9	10.55	27.9	0.479	0.479	49.75	1.143
16	0.39	21.34	13.8	21.34	13.8	0.968	0.968	101.46	2.386
17	0.16	43.74	6.7	43.74	6.7	1.985	1.985	207.04	5.111
18	0.08	123.47	2.4	123.47	2.4	5.602	5.602	416.33	11.338

Table 17: Expected Astrometric and Photometric precision and accuracies for G2 stars *in the 550-850 nm band*. For further details, see the caption of table 14.

V	$N_{e,tot}$	$\delta x^P_{0,S}$	$\delta x^P_{0,S}$	$\delta x^A_{0,S}$	$\delta x^A_{0,S}$	$\delta\pi^P$	$\delta\pi^A$	δV_S	δV_M
	ke^-	mas	1/pix	mas	1/pix	mas	mas	mmag	mmag
(1)	(2)	(3)	(4)	(5)	(6)	(7)	(8)	(9)	(10)
8	692.45	0.40	729.0	0.84	350.0	0.018	0.038	1.38	0.031
9	275.69	0.53	557.0	0.84	350.0	0.024	0.038	2.18	0.049
10	109.82	0.74	399.8	0.84	350.0	0.033	0.038	3.39	0.076
11	43.74	1.09	269.8	1.09	269.8	0.049	0.049	5.20	0.117
12	17.43	1.72	171.4	1.72	171.4	0.078	0.078	8.29	0.187
13	6.95	2.87	102.6	2.87	102.6	0.130	0.130	14.07	0.318
14	2.77	5.10	57.7	5.10	57.7	0.232	0.232	23.61	0.536
15	1.10	9.65	30.5	9.65	30.5	0.438	0.438	46.87	1.075
16	0.44	19.37	15.2	19.37	15.2	0.879	0.879	95.72	2.245
17	0.18	39.44	7.5	39.44	7.5	1.790	1.790	195.83	4.810
18	0.09	107.76	2.7	107.76	2.7	4.889	4.889	395.67	10.670

Table 18: Expected Astrometric and Photometric precision and accuracies for K3 stars *in the 550-850 nm band*. For further details, see the caption of table 14.

V	$N_{e,tot}$	$\delta x^P_{0,S}$	$\delta x^P_{0,S}$	$\delta x^A_{0,S}$	$\delta x^A_{0,S}$	$\delta\pi^P$	$\delta\pi^A$	δV_S	δV_M
	ke^-	mas	1/pix	mas	1/pix	mas	mas	mmag	mmag
(1)	(2)	(3)	(4)	(5)	(6)	(7)	(8)	(9)	(10)
8	921.71	0.38	782.8	0.84	350.0	0.017	0.038	1.20	0.027
9	366.97	0.48	609.6	0.84	350.0	0.022	0.038	1.89	0.042
10	146.18	0.66	446.2	0.84	350.0	0.030	0.038	2.94	0.066
11	58.23	0.96	306.9	0.96	306.9	0.044	0.044	4.51	0.101
12	23.20	1.48	198.6	1.48	198.6	0.067	0.067	7.19	0.162
13	9.25	2.43	121.1	2.43	121.1	0.110	0.110	12.21	0.276
14	3.68	4.24	69.4	4.24	69.4	0.192	0.192	20.50	0.465
15	1.47	7.86	37.4	7.86	37.4	0.357	0.357	40.74	0.932
16	0.59	15.49	19.0	15.49	19.0	0.703	0.703	83.44	1.946
17	0.25	31.06	9.5	31.06	9.5	1.409	1.409	171.69	4.170
18	0.12	78.15	3.8	78.15	3.8	3.546	3.546	350.57	9.255

Table 19: Expected Astrometric and Photometric precision and accuracies for K7 stars *in the 550-850 nm band*. For further details, see the caption of table 14.

V	$N_{e,tot}$	$\delta x^P_{0,S}$	$\delta x^P_{0,S}$	$\delta x^A_{0,S}$	$\delta x^A_{0,S}$	$\delta\pi^P$	$\delta\pi^A$	δV_S	δV_M
	ke^-	mas	1/pix	mas	1/pix	mas	mas	mmag	mmag
(1)	(2)	(3)	(4)	(5)	(6)	(7)	(8)	(9)	(10)
8	1179.04	0.36	828.4	0.84	350.0	0.016	0.038	1.06	0.024
9	469.42	0.45	655.7	0.84	350.0	0.020	0.038	1.67	0.038
10	186.99	0.60	488.0	0.84	350.0	0.027	0.038	2.60	0.058
11	74.48	0.86	341.2	0.86	341.2	0.039	0.039	3.99	0.090
12	29.68	1.31	224.5	1.31	224.5	0.059	0.059	6.36	0.143
13	11.83	2.12	139.1	2.12	139.1	0.096	0.096	10.80	0.244
14	4.71	3.63	81.0	3.63	81.0	0.165	0.165	18.14	0.411
15	1.88	6.62	44.4	6.62	44.4	0.300	0.300	36.10	0.824
16	0.75	12.84	22.9	12.84	22.9	0.583	0.583	74.10	1.721
17	0.31	25.38	11.6	25.38	11.6	1.151	1.151	153.13	3.688
18	0.15	59.14	5.0	59.14	5.0	2.683	2.683	315.29	8.187

Table 20: Expected Astrometric and Photometric precision and accuracies for M2 stars *in the 550-850 nm band*. For further details, see the caption of table 14.

V	$N_{e,tot}$	$\delta x^P_{0,S}$	$\delta x^P_{0,S}$	$\delta x^A_{0,S}$	$\delta x^A_{0,S}$	$\delta \pi^P$	$\delta \pi^A$	δV_S	δV_M
	ke^-	mas	1/pix	mas	1/pix	mas	mas	mmag	mmag
(1)	(2)	(3)	(4)	(5)	(6)	(7)	(8)	(9)	(10)
8	1520.58	0.34	874.5	0.84	350.0	0.015	0.038	0.93	0.021
9	605.40	0.42	703.7	0.84	350.0	0.019	0.038	1.47	0.033
10	241.15	0.55	532.9	0.84	350.0	0.025	0.038	2.29	0.051
11	96.06	0.78	379.0	0.84	350.0	0.035	0.038	3.51	0.079
12	38.27	1.16	253.6	1.16	253.6	0.053	0.053	5.60	0.126
13	15.26	1.84	159.7	1.84	159.7	0.084	0.084	9.52	0.215
14	6.07	3.11	94.7	3.11	94.7	0.141	0.141	15.99	0.362
15	2.42	5.57	52.8	5.57	52.8	0.253	0.253	31.85	0.726
16	0.97	10.62	27.7	10.62	27.7	0.482	0.482	65.51	1.516
17	0.41	20.68	14.2	20.68	14.2	0.938	0.938	135.94	3.248
18	0.19	44.27	6.6	44.27	6.6	2.009	2.009	282.11	7.212

Table 21: Expected Astrometric and Photometric precision and accuracies for M5 stars *in the 550-850 nm band*. For further details, see the caption of table 14.

V	$N_{e,tot}$	$\delta x^P_{0,S}$	$\delta x^P_{0,S}$	$\delta x^A_{0,S}$	$\delta x^A_{0,S}$	$\delta \pi^P$	$\delta \pi^A$	δV_S	δV_M
	ke^-	mas	1/pix	mas	1/pix	mas	mas	mmag	mmag
(1)	(2)	(3)	(4)	(5)	(6)	(7)	(8)	(9)	(10)
8	3073.92	0.30	994.5	0.84	350.0	0.013	0.038	0.66	0.015
9	1223.84	0.35	835.2	0.84	350.0	0.016	0.038	1.04	0.023
10	487.50	0.44	662.8	0.84	350.0	0.020	0.038	1.61	0.036
11	194.19	0.60	494.6	0.84	350.0	0.027	0.038	2.47	0.056
12	77.37	0.85	346.8	0.85	346.8	0.039	0.039	3.94	0.089
13	30.85	1.29	228.7	1.29	228.7	0.058	0.058	6.70	0.151
14	12.28	2.07	142.0	2.07	142.0	0.094	0.094	11.27	0.254
15	4.90	3.54	83.0	3.54	83.0	0.161	0.161	22.50	0.510
16	1.96	6.44	45.7	6.44	45.7	0.292	0.292	46.48	1.066
17	0.82	12.01	24.5	12.01	24.5	0.545	0.545	97.36	2.285
18	0.39	19.95	14.7	19.95	14.7	0.905	0.905	205.78	5.078

On the following pages, the astrometric and photometric precision are tabulated for an **SDSS band**.

Table 22: Expected Astrometric and Photometric precision and accuracies for A0 stars *in an SDSS band with $FWHM_\lambda \approx 130$ nm.* The number of detectable photons is assumed to equal 43% of the astrometric band. A 5 year mission with 180 photometric observations is assumed. For further details, see the caption of table 14.

V	$N_{e,tot}$	$\delta x^P_{0,S}$	$\delta x^P_{0,S}$	$\delta x^A_{0,S}$	$\delta x^A_{0,S}$	$\delta\pi^P$	$\delta\pi^A$	δV_S	δV_M
	ke$^-$	mas	1/pix	mas	1/pix	mas	mas	mmag	mmag
(1)	(2)	(3)	(4)	(5)	(6)	(7)	(8)	(9)	(10)
8	202.78	0.59	501.6	0.84	350.0	0.088	0.127	2.52	0.188
9	80.76	0.82	357.9	0.84	350.0	0.124	0.127	3.90	0.291
10	32.17	1.24	238.1	1.24	238.1	0.186	0.186	6.14	0.459
11	12.82	1.99	147.7	1.99	147.7	0.300	0.300	9.80	0.733
12	5.11	3.45	85.4	3.45	85.4	0.519	0.519	16.52	1.239
13	2.04	6.38	46.1	6.38	46.1	0.960	0.960	29.28	2.209
14	0.81	12.65	23.3	12.65	23.3	1.903	1.903	53.08	4.045
15	0.32	26.59	11.1	26.59	11.1	4.001	4.001	108.94	8.503
16	0.13	56.44	5.2	56.44	5.2	8.493	8.493	217.99	17.838
17	0.06	112.94	2.6	112.94	2.6	16.996	16.996	438.82	39.555

Table 23: Expected Astrometric and Photometric precision and accuracies for G2 stars *in an SDSS band with $FWHM_\lambda \approx 130$ nm.* For further details, see the caption of table 22.

V	$N_{e,tot}$	$\delta x^P_{0,S}$	$\delta x^P_{0,S}$	$\delta x^A_{0,S}$	$\delta x^A_{0,S}$	$\delta\pi^P$	$\delta\pi^A$	δV_S	δV_M
	ke$^-$	mas	1/pix	mas	1/pix	mas	mas	mmag	mmag
(1)	(2)	(3)	(4)	(5)	(6)	(7)	(8)	(9)	(10)
8	231.17	0.56	523.4	0.84	350.0	0.085	0.127	2.36	0.176
9	92.07	0.78	377.1	0.84	350.0	0.117	0.127	3.65	0.272
10	36.68	1.16	253.4	1.16	253.4	0.175	0.175	5.75	0.430
11	14.61	1.85	158.8	1.85	158.8	0.279	0.279	9.18	0.687
12	5.82	3.17	92.7	3.17	92.7	0.478	0.478	15.48	1.161
13	2.32	5.82	50.6	5.82	50.6	0.876	0.876	27.45	2.069
14	0.92	11.43	25.7	11.43	25.7	1.720	1.720	49.79	3.789
15	0.37	23.84	12.3	23.84	12.3	3.588	3.588	102.35	7.966
16	0.15	50.29	5.9	50.29	5.9	7.568	7.568	205.39	16.715
17	0.07	100.21	2.9	100.21	2.9	15.081	15.081	415.68	37.089

Table 24: Expected Astrometric and Photometric precision and accuracies for K3 stars *in an SDSS band with $FWHM \approx 130$ nm.* For further details, see the caption of table 22.

V	$N_{e,tot}$	$\delta x^P_{0,S}$	$\delta x^P_{0,S}$	$\delta x^A_{0,S}$	$\delta x^A_{0,S}$	$\delta\pi^P$	$\delta\pi^A$	δV_S	δV_M
	ke$^-$	mas	1/pix	mas	1/pix	mas	mas	mmag	mmag
(1)	(2)	(3)	(4)	(5)	(6)	(7)	(8)	(9)	(10)
8	273.75	0.53	551.7	0.84	350.0	0.080	0.127	2.17	0.162
9	109.03	0.73	402.6	0.84	350.0	0.110	0.127	3.36	0.250
10	43.43	1.07	274.1	1.07	274.1	0.162	0.162	5.29	0.395
11	17.30	1.69	173.9	1.69	173.9	0.255	0.255	8.44	0.631
12	6.89	2.86	102.9	2.86	102.9	0.430	0.430	14.23	1.067
13	2.75	5.18	56.8	5.18	56.8	0.780	0.780	25.25	1.901
14	1.09	10.05	29.3	10.05	29.3	1.512	1.512	45.84	3.483
15	0.44	20.74	14.2	20.74	14.2	3.121	3.121	94.40	7.322
16	0.18	43.39	6.8	43.39	6.8	6.530	6.530	190.12	15.370
17	0.08	85.97	3.4	85.97	3.4	12.937	12.937	387.32	34.130

Table 25: Expected Astrometric and Photometric precision and accuracies for M2 stars *in an SDSS band with $FWHM_\lambda \approx 130$ nm.* For further details, see the caption of table 22.

V	$N_{e,tot}$	$\delta x^P_{0,S}$	$\delta x^P_{0,S}$	$\delta x^A_{0,S}$	$\delta x^A_{0,S}$	$\delta\pi^P$	$\delta\pi^A$	δV_S	δV_M
	ke$^-$	mas	1/pix	mas	1/pix	mas	mas	mmag	mmag
(1)	(2)	(3)	(4)	(5)	(6)	(7)	(8)	(9)	(10)
8	438.00	0.47	631.2	0.84	350.0	0.070	0.127	1.71	0.128
9	174.45	0.62	477.0	0.84	350.0	0.093	0.127	2.65	0.198
10	69.49	0.87	336.5	0.87	336.5	0.132	0.132	4.18	0.312
11	27.69	1.33	221.3	1.33	221.3	0.200	0.200	6.68	0.499
12	11.03	2.17	135.7	2.17	135.7	0.326	0.326	11.27	0.843
13	4.40	3.79	77.6	3.79	77.6	0.570	0.570	20.01	1.503
14	1.75	7.11	41.4	7.11	41.4	1.069	1.069	36.40	2.754
15	0.70	14.22	20.7	14.22	20.7	2.140	2.140	75.30	5.793
16	0.29	29.02	10.1	29.02	10.1	4.367	4.367	152.97	12.169
17	0.13	56.48	5.2	56.48	5.2	8.500	8.500	316.85	27.070

Astrometric and photometric results for: **FAME Classic.**

Table 26: Expected Astrometric and Photometric precision and accuracies for A0 stars in the **FAME Classic 400-900 nm band**. For further details, see the caption of table 14. For A 2.5 year mission with 1059 astrometric observations on 14 chips is assumed.

V	$N_{e,tot}$	$\delta x^P_{0,S}$	$\delta x^P_{0,S}$	$\delta x^A_{0,S}$	$\delta x^A_{0,S}$	$\delta\pi^P$	$\delta\pi^A$	δV_S	δV_M
	ke$^-$	mas	1/pix	mas	1/pix	mas	mas	mmag	mmag
(1)	(2)	(3)	(4)	(5)	(6)	(7)	(8)	(9)	(10)
8	1848.67	0.23	902.6	0.59	350.0	0.013	0.033	0.986	0.030
9	736.07	0.28	740.8	0.59	350.0	0.016	0.033	1.386	0.043
10	293.12	0.36	572.6	0.59	350.0	0.020	0.033	2.152	0.066
11	116.73	0.50	415.3	0.59	350.0	0.028	0.033	3.159	0.097
12	46.49	0.73	282.5	0.73	282.5	0.041	0.041	5.038	0.155
13	18.52	1.14	180.4	1.14	180.4	0.065	0.065	7.982	0.246
14	7.38	1.90	108.2	1.90	108.2	0.108	0.108	13.472	0.416
15	2.94	3.38	60.9	3.38	60.9	0.191	0.191	22.417	0.696
16	1.17	6.40	32.2	6.40	32.2	0.362	0.362	41.983	1.315
17	0.47	12.92	15.9	12.92	15.9	0.731	0.731	81.937	2.612
18	0.19	27.10	7.6	27.10	7.6	1.532	1.532	164.172	5.433

Table 27: Astrometric and Photometric results for A0 stars in a **FAME Classic SDSS band**. A 2.5 year mission with 75 photometric observations on 1 chip is assumed.

V	$N_{e,tot}$	$\delta x^P_{0,S}$	$\delta x^P_{0,S}$	$\delta x^A_{0,S}$	$\delta x^A_{0,S}$	$\delta\pi^P$	$\delta\pi^A$	δV_S	δV_M
	ke$^-$	mas	1/pix	mas	1/pix	mas	mas	mmag	mmag
(1)	(2)	(3)	(4)	(5)	(6)	(7)	(8)	(9)	(10)
8	407.42	0.33	619.8	0.59	350.0	0.070	0.125	1.822	0.210
9	162.24	0.44	463.1	0.59	350.0	0.094	0.125	2.838	0.327
10	64.62	0.64	324.1	0.64	324.1	0.134	0.134	4.244	0.489
11	25.74	0.97	212.4	0.97	212.4	0.205	0.205	6.771	0.781
12	10.25	1.58	130.4	1.58	130.4	0.334	0.334	10.895	1.258
13	4.09	2.74	75.1	2.74	75.1	0.580	0.580	18.333	2.124
14	1.63	5.09	40.4	5.09	40.4	1.078	1.078	33.002	3.846
15	0.65	10.08	20.4	10.08	20.4	2.132	2.132	62.509	7.373
16	0.26	21.10	9.8	21.10	9.8	4.463	4.463	129.271	15.671
17	0.11	44.20	4.7	44.20	4.7	9.352	9.352	262.437	33.608

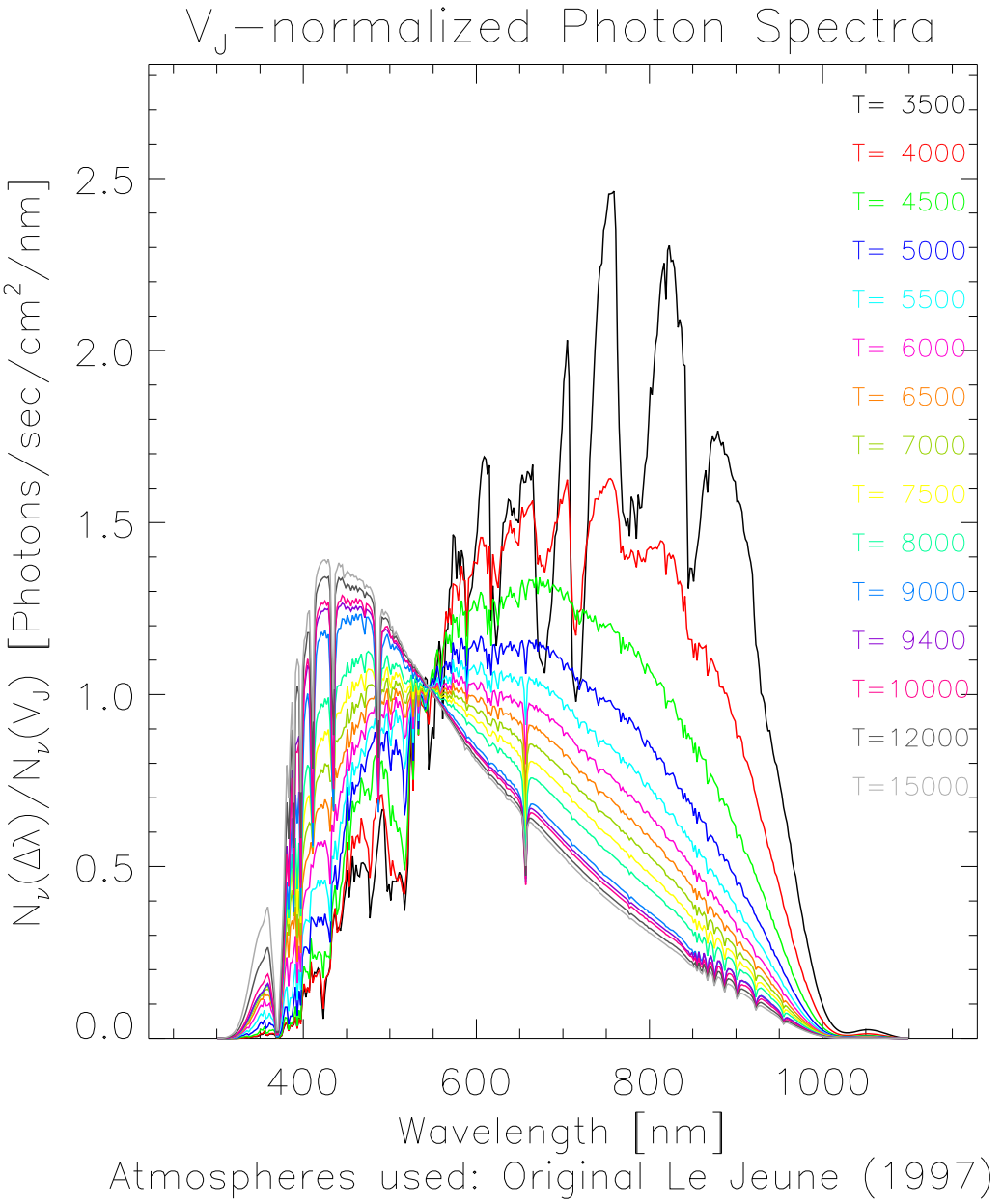

Fig. 1.— The photon spectra for "stars" of various effective temperature, but with the same metallicity ($[Fe/H] = 0$) and surface gravity $log(g)$=4.5]. The spectra are folded with "the" FAME throughput/QE sensitivity curve. The SEDs are scaled to have unit flux in the V band.

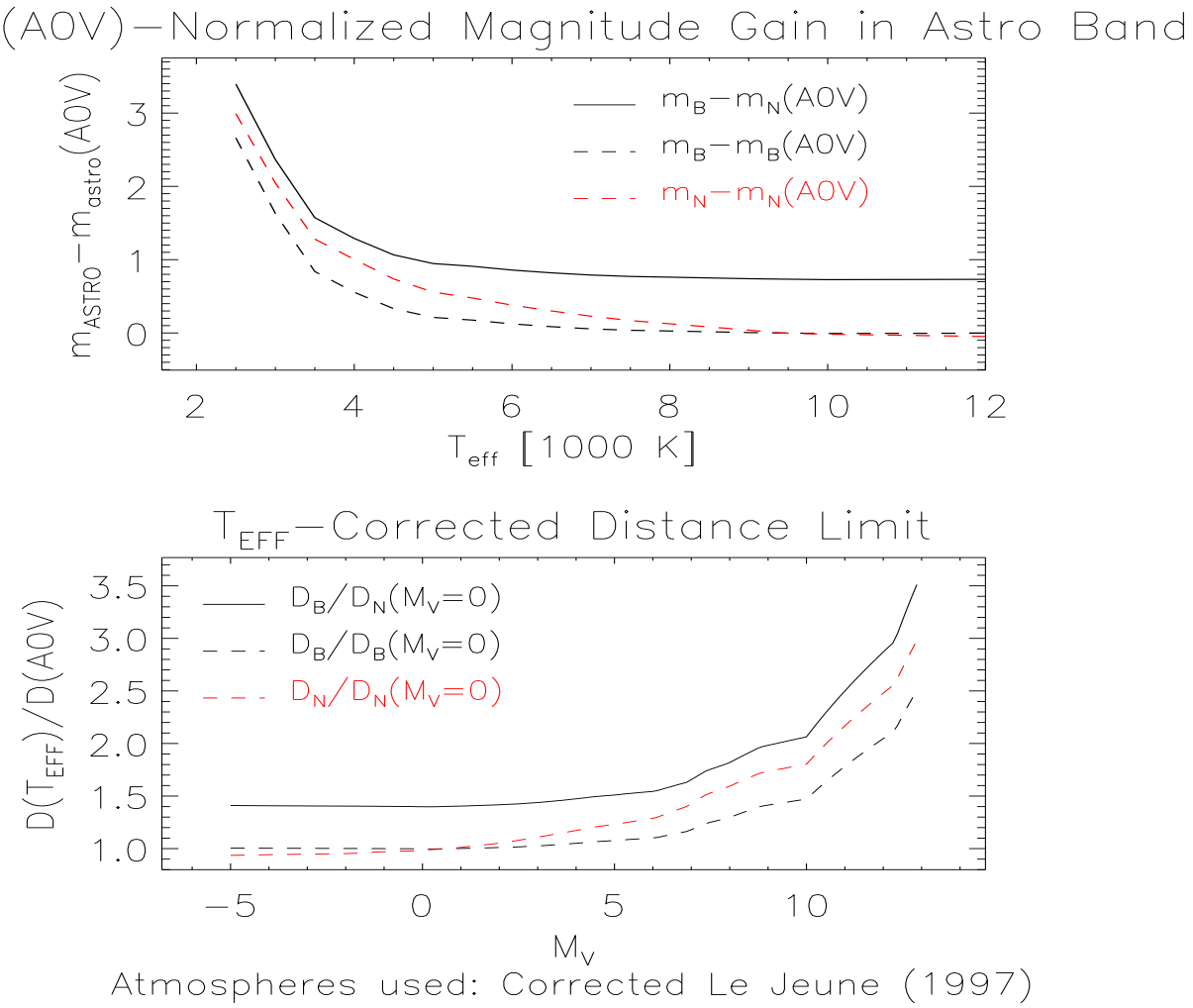

Fig. 2.— In the top panel, I present the apparent magnitude in the astrometric band as a function of effective temperature, normalized by the apparent magnitude of an A0V stars (Vega). All models have *identical* V magnitudes. Three curves are plotted: 1) the magnitude gain of the *broad* astrometric band $[m_B]$ with respect to the magnitude of an A0V star in the *narrow* astrometric band $[m_N(A0V)]$ (full black line), 2) the gain of the *broad* band with respect to the magnitude of an A0V star in the *broad* band $[m_B(A0V)]$ (dashed black line), 3) the gain of the *narrow* band $[m_N]$ with respect to the magnitude of an A0V star in the *narrow* band $[m_N(A0V)]$ (dashed red line [i.e., the "middle" line in both figures]). In the bottom panel I present a transformation of the axes of the upper figure for the same three cases. Here, I converted T_{eff} to absolute magnitude (assuming main-sequence stars), while the magnitude gain corresponds to an increased limiting distance.

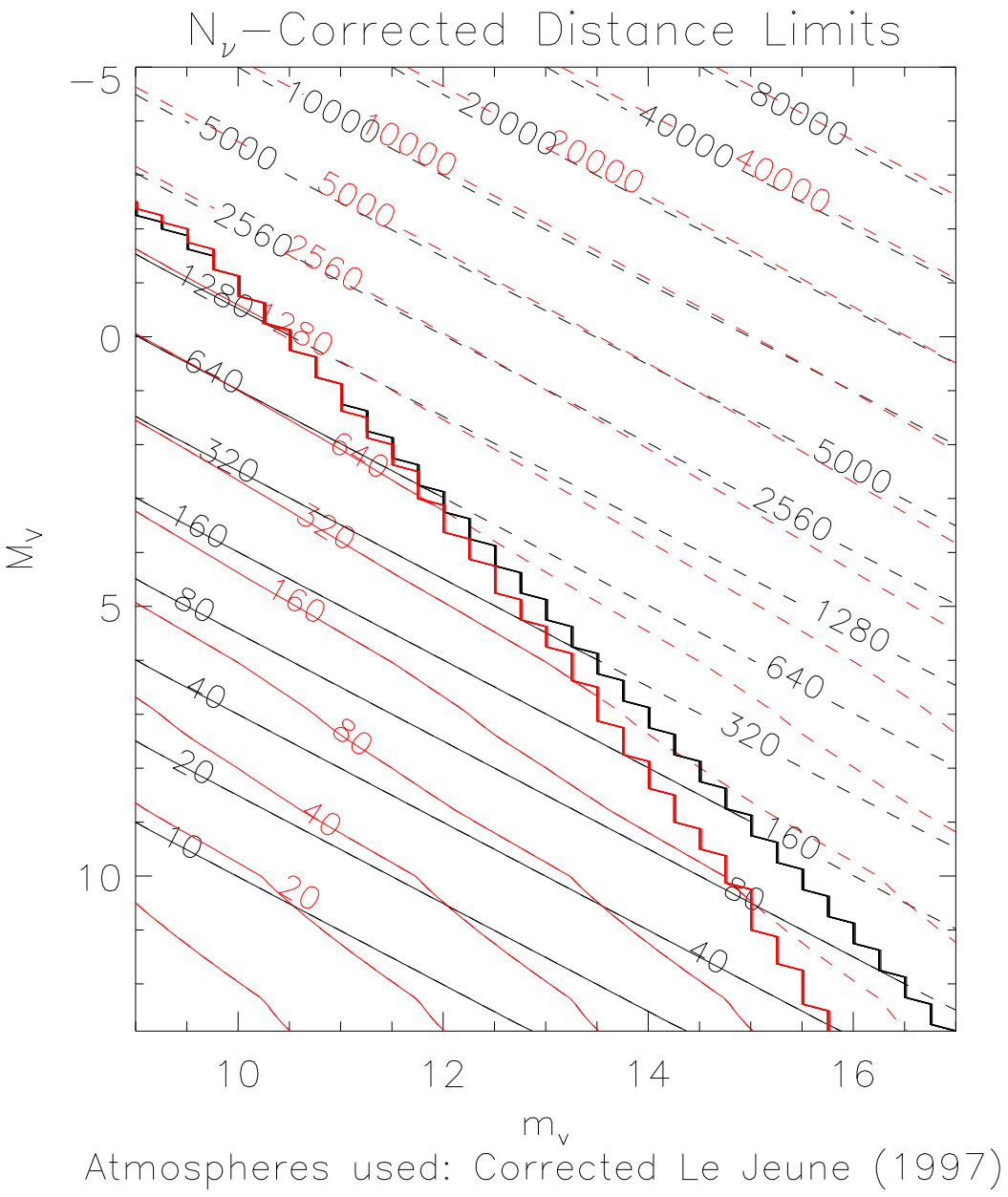

Fig. 3.— Distance as a function of absolute and apparent magnitude assuming no extinction. The straight (black) contours do not include the spectral-type ($=T_{eff}$ = M_V) dependent photon enhancement factors. The curved (red) contours *do* include the $PEF(T_{eff})$ factors correctly. The 10% astrometric distance limit is indicated by the jagged lines. Stars in the region with dashed contours are too far away for meaningful parallax measurements (i.e., distance limited). Both distance limits lines include photon-statistics and readnoise effects.